AD-A217 194

REPORT DOCUMENTATION PAGE

Form Approved
OMB No. 0704-0188

1. AGENCY USE ONLY (Leave blank)	2. REPORT DATE	3. REPORT TYPE AND DATES COVERED
	May 1982	Interim (30 Sept 1980-30 Sept 1981)

4. TITLE AND SUBTITLE
RELATIONSHIPS BETWEEN ELECTRONIC STRUCTURE AND STABILITY OF METALLIC GLASSES.

5. FUNDING NUMBERS
61102F
2306/B2

6. AUTHOR(S)
F. Abeles
M-L. Theye
V. Nguyen Van

7. PERFORMING ORGANIZATION NAME(S) AND ADDRESS(ES)
Universite P. &M. Curie
Laboratoire d' Optique des Solides
Paris, France

AFOSR.TR. 89-1749

8. PERFORMING ORGANIZATION REPORT NUMBER

9. SPONSORING/MONITORING AGENCY NAME(S) AND ADDRESS(ES)
AFOSR
BLDG 410
BAFB DC 20332-6448

10. SPONSORING/MONITORING AGENCY REPORT NUMBER
AFOSR-78-3701

DTIC
ELECTE
JAN 03 1990
S B D

11. SUPPLEMENTARY NOTES

12a. DISTRIBUTION/AVAILABILITY STATEMENT
Approved for public release;
distribution unlimited.

12b. DISTRIBUTION CODE

13. ABSTRACT (Maximum 200 words)
Amorphous metallic Ag-Ge alloy films were obtained by co-evaporation on cold substrates for Ge concentrations between 20 and 40 at.% . Their stability versus temperature, as well as the structural rearrangements occurring during annealing, are studied by in situ resistance measurements and room-temperature electron diffraction experiments. The d.c. electrical resistivity and the complex dielectric constant (between 0.6 and 4 eV) of the as-deposited amorphous alloys are investigated in detail. We show that a simple Drude model satisfactority accounts for their optical properties, at least for Ge concentrations between 20 and 30 at.%. The values of the free-electron parameters are discussed and compared to those already obtained for amorphous Au-Ge alloys.

14. SUBJECT TERMS			15. NUMBER OF PAGES 37
			16. PRICE CODE
17. SECURITY CLASSIFICATION OF REPORT	18. SECURITY CLASSIFICATION OF THIS PAGE	19. SECURITY CLASSIFICATION OF ABSTRACT	20. LIMITATION OF ABSTRACT
unclassified	unclassified		

NSN 7540-01-280-5500

Standard Form 298 (890104 Draft)
Prescribed by ANSI Std. 239-18
298-01

Grant Number : AFOSR-78-3701

RELATIONSHIPS BETWEEN ELECTRONIC STRUCTURE AND STABILITY OF METALLIC GLASSES

F. Abelès
M.L. Thèye
V. Nguyen Van

Laboratoire d'Optique des Solides
Université Pierre et Marie Curie
4 place Jussieu
75230 Paris Cedex 05
France

May 1982

Interim Scientific Report, 30 September 1980 - 30 September 1981

Prepared for

United States Air Force, Air Force Office of Scientific Research, Building 410, Bolling AFB, D.C. 20332, U.S.A.

and

European Office of Aerospace Research and Development, London, England.

Table of contents

This year has been dedicated to thorough investigations of the electronic properties of amorphous metallic Ag-Ge alloys. These alloys are similar to the Au-Ge alloys studied previously, but in Ag the d-band is located at lower energies with respect to the Fermi level than in Au. The hybridization between the Ge s,p-states and the noble metal d-states may therefore occur differently; moreover, this extends the energy range over which the free-electron behaviour of the optical properties can be studied. Amorphous metallic Ag-Ge alloys have been obtained by co-evaporation onto cold substrates for Ge concentrations ranging from 20 to 40 at. %. We have controlled their stability as a function of temperature and we have followed the crystallization processes by in-situ resistance measurements. We have determined their transport properties and we have analyzed their optical properties according to the free-electron Drude model. We discuss the variation of the conduction electron parameters with composition and we compare the results with those already obtained for the Au-Ge alloys.

1.- Experiment.

The samples are thin (200-400 Å) films deposited under ultra-high vacuum (base pressure 10^{-9} Torr, rising to 5.10^{-8} Torr during evaporation) onto well-polished glass or silica substrates maintained at low temperature (15-20 K), by co-evaporation of the two constituents from two separate tungsten crucibles (Fig.1). The evaporation rate of each crucible is controlled with a calibrated quartz microbalance connected to a minicomputer Apple II Plus which commands and regulates the crucible heating. This system allows us to mon[illegible] both the composition and the thickness of the film with an uncertain[illegible] ±1 %. As a check, the film thickness is subsequently measured at room temperature by an X-ray interference method (1). The total deposition rate is of the order of 10 Å/sec.

A specially-built spectrophotometer (2) (Fig.2) allows to measure in situ, at the deposition temperature, the transmittance T

and relectance R of the film at near normal incidence, between 0.6 and 4.5 eV (2.0-0.3 μm). The film d.c. electrical resistance is also measured by a four-points method. The temperature of the film can then be varied over the range 15-300 K, the optical measurements being repeated in situ at any desired temperature. Resistance measurements as a function of temperature allow to determine the range of stability of the as-deposited sample (reversible variation) and to follow possible structural changes during annealing (irreversible variation). A special set-up (Fig.3) is used in order to measure resistance changes as small as 10^{-3} Ω for resistance values greater than 100 Ω ; this is necessary in order to determine the temperature coefficient of the resistance of the amorphous alloys which is extremely small ($\sim 10^{-5}$ K^{-1}), accurately enough.

The structure of the samples is investigated at room temperature by electron microscopy and electron diffraction on pieces detached from the substrate with collodion. As we shall see, all samples are at least partly crystallized at room temperature. These results are nevertheless used, together with the annealing curves (variation of resistance versus temperature), to infer the structure of the as-deposited samples, as well as the structural changes occurring upon annealing.

2.- Existence and stability of amorphous metallic Ag-Ge alloys.

The Ag-Ge system exhibits a eutectic for $x_{Ge} \simeq 24.1$ at % (3); the solid solubility of Ag in Ge is negligible, that of Ge in Ag is small : 9.6 at % at the eutectic temperature, 924 K (4) (Fig.4). Although the eutectic is less deep than that in the Au-Si system, or even in the Au-Ge system, it is expected that amorphous alloys can be obtained under appropriate preparation conditions. The predominance of hetero-atomic interactions in the liquid Ag-Ge eutectic, as deduced from neutron diffraction experiments (5), favours such a possibility.

We have investigated Ag-Ge films deposited by co-evaporation on cold substrate as explained above, with Ge concentrations varying from 20 to 40 %. The d.c. electrical resistivity ρ_e of these films at the deposition temperature is of the order of 100-200 μΩcm, and its temperature coefficient $\frac{1}{\rho_e} \cdot \frac{d\rho_e}{dT}$ is very small (of the order of 10^{-5} - 10^{-4} K^{-1}) and negative except for $x_{Ge} = 20.5$ at %. The opti-

cal properties of these films in the near infra-red exhibit a metallic behaviour, with values of the conduction electron parameters very typical of amorphous metallic alloys, as we shall see. All these observations strongly suggest that we obtained amorphous metallic alloys for all compositions investigated. However, this assumption cannot be confirmed by the electron microscope investigations, because all samples are partly crystallized at room temperature. Figure 5 shows for example an electron micrograph (a) and an electron diffraction diagram (b) for a film (d = 205 Å) with $x_{Ge} = 26.5$ at %. A large number of very small crystallites can similarly be detected in all films investigated. The corresponding strong diffraction peaks occur in the same s regions where the diffuse diffraction pattern of the amorphous metallic alloy phase is expected; it is therefore very difficult to decide whether such a phase is still present at room temperature. However, one can observe a broad halo which is approximately centred at the same s value as the first diffuse ring characteristic of covalent amorphous Ge. This can clearly be seen on figure 6, which shows densitograms of the diffraction patterns for three different compositions. This halo is not present or appears very faintly for small Ge concentrations, but it becomes more and more pronounced as the Ge content increases. The presence of amorphous-Ge-like rings was also detected in the Au-Ge case, but only for high Ge concentrations (6). It can be attributed to the existence of covalent Ge-Ge local environments, which can result from the structural rearrangements occuring upon annealing, or which can already be present in the as-deposited films under certain deposition conditions. One must notice that Ge-Ge covalent bonds seem to form more easily in the Ag-Ge case than in the Au-Ge case, which can be related to the poorer stability of the Ag-Ge amorphous metallic alloys.

As for the crystalline phases which appear upon annealing to room temperature, the diffraction diagrams clearly show the main lines characteristic of face centred cubic Ag, i.e. (111), (220) and (311) (and also (200) in some cases)(Fig.6). However, additional strong diffraction peaks which can systematically be observed on either side of the (111) Ag line, although with variable relative intensities (indicated by arrows in figure6), as well as fainter structures appearing at larger s values, probably indicate the presence of an hexagonal close-packed alloy crystalline phase. This phase could correspond to that already obtained by rapid cooling from the liquid state (7) for Ge

concentrations between 10 and 30 %, the range of homogeneity being 20-22 at. % and the lattice parameters : a ≃ 2.90 Å and c ≃ 4.72 Å (from our own data, the c value should be slightly larger). Crystalline Ge only appears for higher annealing temperatures, as shown by figure 7. This densitogram shows, besides the lines corresponding to pure Ag and pure Ge, several lines confirming the existence of an hexagonal alloy phase.

Figure 8 shows the variation of the d.c. electrical resistivity ρ_e versus temperature during annealing from the deposition temperature (15-20 K) to room temperature, for several films with increasing Ge concentrations. An arrow indicates in each case the temperature at which the $\rho_e(T)$ variation ceases to be reversible. The temperature range of (meta)stability of the as-deposited samples determined in this way depends on the composition but is very limited for all alloys. As for the irreversible part of the $\rho_e(T)$ curves, at higher temperatures, different results are obtained depending on the film composition. In all cases, a more or less steep drop when approaching room temperature indicates the beginning of the crystallization. But at intermediate temperatures, the $\rho_e(T)$ behaviour is strikingly modified as the Ge concentration increases. For small Ge contents ($x_{Ge} = 20.5$, 25, 26.5 at. %), ρ_e varies very little; it first decreases slightly, then remains approximately constant or exhibits a faint increase. It is interesting to notice that, for $x_{Ge} = 25$ at. % , which is very close to the eutectic composition, the overall variation of ρ_e between 20 K and 270 K is remarkably small, suggesting very reduced annealing effect. For high Ge contents ($x_{Ge} = 29.6$, 37 at. %), on the contrary, ρ_e increases significantly and goes through a sharp maximum before dropping when the crystallization starts. Similar observations were already made during annealing of co-evaporated amorphous metallic Au-Si (8), Au-Ge (6) and (AgCu)-Ge (9) alloys. These differences in the annealing behaviour according to the alloy composition indicate that the processes of atomic rearrangement are not the same in all cases. For small Ge concentrations, only relaxation of the amorphous structure must take place, without drastic changes of short-range order. For large Ge concentrations, more important modifications of the local atomic environments probably occur, which can lead to the formation of Ge-Ge covalent bonds. This would explain the amorphous-Ge-like broad halos observed on the diffraction patterns. Such a process could also

happen to a certain extent in films with smaller Ge contents, when favoured by composition fluctuations or structure inhomogeneities under certain deposition conditions.

3.- d.c. electrical resistivity of amorphous metallic alloys.

As already emphasized, the d.c. electrical resistivity ρ_e at deposition temperature of the Ag-Ge films is large, of the order of 100-200 μΩcm, and it increases with the Ge concentration (figure 8). In the range of (meta)stability of the as-deposited alloys, the resistivity decreases roughly linearly with temperature for all films except the more dilute one ($x_{Ge} = 20.5$ at.%). The absolute value of its temperature coefficient $\alpha = \frac{1}{\rho_e} \cdot \frac{d\rho_e}{dT}$ is always very small ($10^{-5} - 10^{-4}$ K^{-1}) but it increases slightly with increasing the Ge concentration. These results are summarized in table I and figure 9a and b, for Ge concentrations between 20 and 40 at. %. One can see that α goes through zero for $x_{Ge} \simeq 23$ at. %. The alloy with $x_{Ge} = 32$ at. % has both a low resistivity and a small temperature coefficient (in absolute value) when compared to the other alloys; this difference (which is also found in the optical properties) can be due to the fact that this alloy has a more relaxed structure, because of favourable deposition conditions.

These data for amorphous metallic Ag-Ge alloys are very similar to those reported for $(Ag_{0.5}Cu_{0.5})_{1-x}$ Ge_x amorphous alloys (9) taken at room temperature; in this case however, α becomes negative at a smaller Ge concentration (≃ 10 at. %) and its absolute values are somewhat larger. One can also notice that the ρ and α values which we obtained at low temperature (20K) for similarly co-evaporated amorphous Au-Ge alloys in previous studies (10) were very close to the present values : for example, for x_{Ge} = 24 at. % , ρ_e = 121 μΩcm and $\alpha = -4.10^{-5}$ K^{-1}.

According to the Ziman theory (11) developed for simple liquid metals, a negative temperature coefficient of the resistivity is observed when the ration $2k_F / K_p$, where $2k_F$ is the diameter of the Fermi sphere, and K_p is the wavenumber corresponding to the first peak in the static structure factor (in the diffraction diagram), is close to unity. In fact, it has been shown that this ratio

falls between 0.95 and 1.1 for a variety of simple liquid metals and alloys (12). The extension of the Ziman theory to the electron transport properties of amorphous alloys has been attempted recently by various authors (13-16). This extended Ziman theory predicts that the electrical resistivity changes linearly with temperature in the range above about a half of the Debye temperature, the sign of this variation depending on the ratio $2k_F / K_p$. At low temperatures, the theory predicts a T^2 dependence.

One of the difficulties in testing the validity of the extended Ziman theory for amorphous metallic alloys lies in the evaluation of $2k_F$. In the case of Ag-Ge or parent alloys, where a quasi-free electron model is expected to hold, a reliable estimation of this quantity becomes possible. We shall see in the next paragraph that the analysis of the optical properties in terms of the Drude model allows to determine the effective number of conduction electrons per unit volume N_{eff}, from which $2k_F$ can be deduced in a straightforward manner :

$$2 k_F = 2 \left[3 \pi^2 N_{eff} \right]^{1/3}$$

Unfortunately, as we emphasized in paragraph 2, we were unable to determine K_p, i.e. the position of the first maximum in the diffraction diagram of the amorphous alloys, since all our samples were at least partly crystallized at room temperature. We can however assume that the value of K_p in amorphous Ag-Ge alloys is equal to that in liquid Ag-Ge alloys for the same composition, as verified in the Au-Ge case (6); this gives $K_p = 2.65$ Å^{-1} at the eutectic composition $x_{Ge} = 24.1$ at. % (5); K_p varies little with composition in the range investigated. We shall come back to the evaluation of the $2k_F / K_p$ ratio in paragraph 5, when discussing the free-electron model for the electronic structure of the amorphous Ag-Ge alloys. On the other hand, the temperature range of stability of our Ag-Ge alloys was too small to allow the determination of the exact temperature dependence of their electrical resistivity both below and above the Debye temperature.

One must recall that detailed studies of amorphous $(Ag_{0.5} Cu_{0.5})_{1-x} Ge_x$, for which a simple free electron model is claimed to be valid (9,17), with Ag, Cu and Ge contributing with 1, 1 and 4

electrons per atom to the conduction band respectively, have shown that the temperature coefficient of their resistivity becomes negative for $2k_F / K_p = 0.95$; this is in good agreement with the results on Cu-Ge liquid alloys for example, and lends support to the validity of the Ziman theory for these amorphous alloys. However, α remains negative even when $2k_F / K_p$ approaches 1.1 , which is in contradiction with the liquid case, where α becomes again positive. Similar tendency has also been found in Mg-Zn amorphous alloys (18).

4.- Optical properties of amorphous metallic Ag-Ge alloys.

4.1.- Description of the optical data.

Figure 10 shows the reflectance (R) and transmittance (T) curves as a function of wavelength between 0.30 and 2.0 μm for a 207 Å Ag-Ge film with x_{Ge} = 25 at. %, as-deposited (deposition temperature 20 K) (a), and annealed at 120 K (b) and at room temperature (c). These spectra are strikingly featureless, even at short wavelengths where the sharp R minimum and T maximum at about 0.32 μm characteristic of pure Ag cannot be detected, even after annealing at room temperature. Annealing has practically no effect on the R and T values in the near infra-red, it only modifies slighty the curvature of the spectra in the visible.

The complex dielectric constant $\tilde{\varepsilon} = \varepsilon_1 + i\varepsilon_2 = (n + ik)^2$ is determined from the measured R and T values at each wavelength, using exact thin film formulae (19) and taking into account multiple reflections in the transparent substrate. Very accurate optical measurements are necessary, especially in the near infra-red, in order to obtain reliable $\tilde{\varepsilon}$ values. We are indeed in a case where, when trying to solve the system of two equations with two unknowns :

$$R(n, k) = R_{ex}$$

$$T(n, k) = T_{ex}$$

very small experimental errors on R and T can lead to very large uncertainties on n and k , or even to no solution at all. The estimated accuracy on our R and T measurements is of the order of 1 - 2 per mil.

Figure 11 shows the optical absorption ε_2 / λ versus energy,

as determined at the deposition temperature (15-20 K), for several Ag-Ge films with Ge concentrations from 20.5 to 32 at. %. The spectrum for pure crystalline Ag at room temperature (20) is also shown for comparison. Striking differences are at once noticed between the alloys and the pure matrix. The optical absorption of the alloys is much higher, especially in the near infra-red. Moreover, while in pure Ag a steep absorption edge indicates the onset of interband transitions from the top of the d-band to the conduction band at the Fermi level ($\hbar\omega_i$ = 3.86 eV (20)), in the alloys there is no indication of such an absorption edge, at least in the spectral range investigated. The overall shape of these spectra looks very similar to that observed for amorphous metallic Au-Si (21) and Au-Ge (10) alloys.

4.2.- Analysis of the optical data.

We have attempted to analyze the dielectric constant of the as-deposited Ag-Ge films with a quasi-free electron model. The (ε_1 , ε_2) data were tentatively fitted with the Drude expression :

$$\tilde{\varepsilon} = 1 - \frac{\omega_p^2}{\omega\left(\omega + \frac{i}{\tau_o}\right)} + \delta\varepsilon_1{}^i$$

where $\omega_p = (4\pi N_{eff} e^2 / m_o)^{1/2}$ (N_{eff} the effective number of electrons per unit volume and m_o the optical effective mass) is the plasma frequency of the quasi-free conduction electrons and τ_o their optical relaxation time. The constant real term $\delta\varepsilon_1{}^i$ accounts for the contribution of possible interband transitions occurring at higher energies. One can also write :

$$\varepsilon_1 = P - \frac{\lambda^2}{\lambda_o{}^2 \left(1 + \left(\frac{\lambda}{\lambda_\tau}\right)^2\right)}$$

$$\varepsilon_2 = \frac{\lambda^3}{\lambda_o{}^2 \lambda_\tau} \quad \frac{1}{1 + \left(\frac{\lambda}{\lambda_\tau}\right)^2}$$

where λ_o and λ_τ are the wavelengths corresponding to ω_p and τ_o respectively, and $P = 1 + \delta\varepsilon_1{}^i$. The three parameters to be adjusted were λ_o , λ_τ and P , which also means : N_{eff} , τ_o and $\delta\varepsilon_1{}^i$;

m_c was taken to be equal to the free electron mass for simplicity. We have also used a slightly more sophisticated model, in which the optical relaxation time τ_o is allowed to vary with frequency, according to (22) :

$$\frac{1}{\tau_o} = \frac{1}{\tau_o^o} + a.\,\omega^2 \quad \text{or} \quad \frac{1}{\lambda_\tau} = \frac{1}{\lambda_\tau^o} + \frac{b}{\lambda^2}$$

In this model, we have four adjustable parameters λ_o , λ_τ , b and P, which also means : N_{eff} , τ_o^o , a and $\delta\varepsilon_1^i$. Since a free-electron-like behaviour seems to be obeyed over a large spectral range in the Ag-Ge system, the range of (ε_1 , ε_2) values used for the fitting procedure was varied in order to check the reliability of the results. In the same spirit, not only the (ε_1 , ε_2) values, but directly the (R, T) values, were fitted with the Drude model, in order to get rid of the uncertainties in the $\tilde{\varepsilon}$ determination.

Table II presents the results of several fits on (R , T) and (ε_1 , ε_2) with the two models for a 207 Å Ag-Ge film with x_{Ge} = 25 at. %; the root mean square deviation per point Σ is also indicated in each case. Figures 12 and 13 show a comparison of the experimental data and of the values deduced from some of these fits, for (R , T) and (ε_1 , ε_2) respectively. One can make the following comments :

i) when the fitting procedure is applied to the data in the large-wavelength range, say from 2.0 to about 0.7 - 0.6 µm, the simple Drude model with a constant relaxation time reproduces the data quite satisfactorily. Figure 13 shows that the agreement is perfect on both ε_1 and ε_2 from 0.6 to about 1.7 eV, and that, for higher energies, the experimental values of ε_2 deviate upwards with respect to the model; the agreement is however still good for ε_1.

ii) when the fitting procedure is applied to the data in a larger spectral range, say from 2.0 to 0.4 µm, the values of the parameters are not significantly modified but the root mean square deviation per point Σ increases strongly. This confirms that the optical properties strictly follow the simple Drude model at low energies only, up to about 1.7 eV.

iii) the quality of the fit attempted over a large spectral range (from 2.0 to 0.4 µm for example) is not improved if the optical relaxation time is allowed to vary with frequency. Therefore, such a τ_o va-

riation does not explain the deviation observed at high energies between the ε_2 experimental values and the simple Drude model. Besides, one must notice that, if $\frac{1}{\tau_o}$ is determined by the expression derived from the Drude formulae :

$$\frac{1}{\tau_o} = 2\pi c \quad \frac{\varepsilon_2 / \lambda}{\varepsilon_1 - P}$$

(taking a reasonable value for P), then fairly constant values are obtained from 0.6 to about 1.5 eV (Fig.14).

Similar conclusions can be deduced from the analysis of the optical properties of all the Ag-Ge films with compositions close to the eutectic composition : $20 \lesssim x_{Ge} < 30$ at. %. A Drude model with a constant relaxation time allows to reproduce the near infra-red data quite satisfactorily up to about 1.7 eV. At higher energies, an additional contribution to the optical absorption is systematically observed; it increases smoothly with increasing energy. The same result was already obtained in the study of Au-Ge alloys (10). In this case, the extra-absorption was attributed to interband transitions; the fact that the absorption edge was so gradual when compared to that in pure Au, was taken as an evidence that in the alloys the Au d-states were hybridized with the Ge s,p-states. In the Ag-Ge case, it seems from X-ray photoemission experiments (23) that the mixing of the Ag d-orbitals with the Ge s and p-orbitals is not so large. On the other hand, it is surprising that no reminiscence of the pure Ag interband absorption edge can be detected in the data. Of course, measurements at higher energies are necessary in order to determine whether such an edge has been shifted by a displacement of the Fermi level with respect to the Ag d-band, or is really washed out in the amorphous alloys.

For Ag-Ge films with higher Ge concentrations : $x_{Ge} \simeq 30$ - 35 at. %, although the optical spectra look very similar, the results of the fitting procedure with the Drude model are much less clear. Although the root mean square deviation per point Σ remains reasonable in all cases, the values of the adjusted parameters vary rather strongly with the (R , T) or (ε_1 , ε_2) range chosen for the fit. At the moment, we cannot decide whether these discrepancies are due to experimental errors in the data, the influence of which would be

larger in these cases, or whether they are really indicative of the inadequacy of the Drude model for more concentrated alloys. One must recall that the annealing behaviour of these alloys is peculiar (see figure 8) and suggests the formation of covalent Ge-Ge bonds. These alloys may already present some inhomogeneity at the deposition temperature, for example different types of local environments corresponding to microscopic composition fluctuations. This inhomogeneity may affect the film optical properties, while modifying very little the electrical resistivity behaviour.

The values of the characteristic parameters of the conduction electrons for the most concentrated alloys must therefore be considered with caution. We preferred to retain the values obtained by a fit over a large spectral range (from 2 to 0.5 - 0.4 μm), because they allowed to reproduce the whole (ε_1 , ε_2) data in a rather satisfactory manner.

5.- Discussion of the free-electron model.

Table III presents the values of the characteristic parameters of the conduction electrons, the effective number per unit volume N_{eff} and the optical relaxation time τ_o , as deduced from the analysis of the complex dielectric constant in terms of the simple Drude model, for a few Ag-Ge alloys with different compositions. One has also indicated the values of the average effective number of conduction electrons per atom n_{eff} , defined by :

$$n_{eff} = \frac{N_{eff}\, D}{\mathcal{N}.\, A}$$

where D is the density and A the average atomic weight ($A = 107.87\ (1-x) + 72.59\ (x)$) of the particular alloy and $\mathcal{N}$ is the Avogadro number. We do not know the density of our co-evaporated amorphous alloys. However, density measurements performed on flash-evaporated amorphous ($Ag_{0.5}Cu_{0.5}$)-Ge alloys have shown that the ratio $\frac{D}{A}$ increases only very slightly when the Ge concentration increases (9); a similar result has been obtained for co-evaporated amorphous Au-Si alloys (8). To a first approximation, we therefore considered the ratio $\frac{D}{A}$ as a constant, equal to the value for pure Ag. Table III also gives the values of the "optical" resistivity ρ_o

deduced from the optical characteristic parameters N_{eff} and τ_o by :

$$\rho_o = N_{eff} e^2 \frac{\tau_o}{m}$$

where m is taken as equal to the free electron mass; these values of ρ_o must be compared to the values of the d.c. electrical resistivity ρ_e . For completeness, we have reported in table III the values of the same quantities for two amorphous Au-Ge alloys with compositions close to the eutectic composition (which is $x_{Ge} = 27$ at. % in this case).

One can make the following comments on these results :

a) the average effective number of conduction electrons per atom n_{eff} increases with the Ge concentration for both the Ag-Ge and Au-Ge alloys. It is interesting to compare the experimental values with those calculated according to a simple model where Ag or Au and Ge would donate 1 and 4 electrons per atom respectively to the conduction band of the alloy :

$$n_o = 4x + (1 - x)$$

Indeed, Ge has four valence electrons, which behave like quasi-free conduction electrons when Ge is in its metallic state; the analysis of the optical properties in terms of the Drude model for liquid Ge yields $n_{eff} = 4.3$ (24). The values of n_o are indicated between parentheses in table III.

In the case of Ag-Ge alloys, one can see that, for small Ge concentrations, close to the eutectic one ($x_{Ge} = 20.5$, 25, 26.5 at. %), the experimental values of n_{eff} are close to the computed values n_o , although slightly smaller. The difference, of the order of 10 %, may be accounted for by errors in the optical data and uncertainties in the analysis in terms of the Drude model. One can therefore conclude that the simple free-electron model described above is roughly verified for the amorphous Ag-Ge alloys, like for the amorphous $(Ag_{0.5}Cu_{0.5})$-Ge alloys (9,17). In the case of the Au-Ge alloys, for the smallest Ge concentration ($x_{Ge} = 24$ at. %) the experimental value of n_{eff} is also rather close to the computed value, but slightly larger. We do not think that this discrepancy with respect to the Ag-Ge case is due to experimental errors. It should

indicate that the electronic structure of Au-Ge alloys is less simple, certainly because of the hybridization between the Ge s,p-states and the Au d-states; additional electrons, probably with d character, must contribute to the conduction band. One must recall that such an hybridization has been predicted theorically (25) and leads to an anti-resonance structure in the p- and s-density of states of the alloy.

For higher Ge concentrations, in both types of alloys the experimental values of n_{eff} become significantly larger than the computed values n_o. This may indicate that hybridization effects become more important as the Ge content increases. However, we have already emphasized that the validity of the Drude model is then questionable, probably because of inhomogeneities of the samples accompanied by local modifications of the bonding character. This would be particularly true in the Ag-Ge case, where Ge shows a greater tendency to give up the metallic bonding into which it is forced by the environment of Ag atoms, and to take its more natural (in the solid state) covalent bonding.

b) the optical relaxation time τ_o is extremely small and decreases as the Ge content increases. For comparison, in crystalline pure Ag at room temperature, τ_o is two orders of magnitude larger (20); in liquid Ag, it is still one order of magnitude larger (26). However, in liquid Ge, the τ_o value is comparable, of the order of 10^{-16} sec. (24). Such very small values of the optical relaxation time are typical of amorphous metallic alloys and have already been obtained for Au-Si (21) and Au-Ge (10) alloys. They are not surprising since the resistivity of these alloys is very high compared to that of crystalline pure metals and most crystalline alloys. They correspond to extremely short mean free paths ℓ given by :

$$\ell = v_F \cdot \tau_o$$

where v_F is the Fermi velocity of the conduction electrons, which, in a free-electron model, can be deduced from the effective number of conduction electrons per unit volume N_{eff} by :

$$v_F = \frac{h}{m} \left(\frac{3}{8\pi} N_{eff} \right)^{1/3}$$

(m is the free electron mass and h the Planck constant). For example, the mean free path ℓ would be equal to 6.10 Å for the Ag-Ge

alloy with $x_{Ge} = 20.5$ at. %, and to 4.36 Å for the Ag-Ge alloy with $x_{Ge} = 26.5$ at. %; this is of the order of the interatomic distances. In such conditions, one may question the validity of a free-electron model, both for the optical and the transport properties of these alloys.

c) the "optical" resistivity ρ_o is very close to the d.c. electrical resistivity ρ_e. The difference may be accounted for by experimental uncertainties on the optical data. This is an important result, since it proves the consistency between the directly measured resistivity, and the resistivity deduced from the optical properties by a free-electron analysis. It confirms that, at least to a first approximation, a free-electron model can be applied in order to account for the "metallic properties" of the amorphous alloys.

One must recall that, in crystalline pure metals, the optical resistivity is usually found to be larger than the electrical resistivity; for example in Ag, $\frac{\rho_o}{\rho_e} \simeq 2$ (20). This can be explained by the anisotropy of the Fermi surface. In crystalline alloys, the ratio tends to be closer to unity, for example in alloys between noble metals (27); this is consistent with a reduction of anisotropy effects in compositionally disordered alloys. In amorphous alloys, the ration $\frac{\rho_o}{\rho_e}$ is also expected to be close to unity. As already emphasized, we attribute the deviations from unity which we obtained for Ag-Ge and Au-Ge alloys to experimental uncertainties in both the optical data and their analysis.

d) as emphasized in paragraph 3, we can determine the diameter of the Fermi sphere $2k_F$ from the experimental values of the effective number of conduction electrons per volume unit N_{eff}. We find $2k_F = 2.73$, 2.73 and 2.83 $Å^{-1}$ for the Ag-Ge alloys with $x_{Ge} = 20.5$, 25 and 26.5 at.% respectively. The corresponding values of the ratio $\frac{2k_F}{K_p}$ are : 1.03, 1.03 and 1.07. At least for the last two alloys, for which the temperature coefficient of the resistivity is negative, these values, close to unity, are in agreement with the assumption of the Ziman theory. However, for the Ag-Ge alloy with $x_{Ge} = 32$ at.%, α is still negative, while the ration $\frac{2k_F}{K_p}$ is already equal to 1.2. Therefore, the extended Ziman theory is certainly less adequate for amorphous alloys than for liquid alloys. A different theory has recently been proposed (28), which takes into account the structural "indeterminacy" in the atomic arrangement of amorphous alloys; the electron transport can be understood in terms of an attractive interaction between conduc-

tion electrons and localized excitations arising from this indeterminacy. Further transport measurements are now necessary in order to test this theory.

REFERENCES

1.- H. KIESSIG, Ann.Phys. (Leipzig) 10, 769 (1931);
W. UMRATH, Z.Angew.Physik 22, 406 (1967).

2.- V. NGUYEN VAN and S. FISSON, Rev.Phys.Appl. 13, 155 (1978).

3.- R. HULTGREN, P.D. DESAI, D.T. HAWKINS, M. GLEISER and K.K. KELLEY, Selected Values of Thermodynamic Properties of Binary Alloys, American Society for Metals, Metals Park, OH, 1973.

4.- E.A. OWEN and V.W. ROWLANDS, J.Inst.Met. 66, 361 (1940).

5.- M.C. BELLISSENT-FUNEL, P.J. DESRE and G. TOURAND, J.Phys.F. 7, 2485 (1977).

6.- V. NGUYEN VAN, S. FISSON and M-L. THEYE, Proc. 8th Int. Vacuum Congress, Cannes, 1980, in Vide, Couches Minces, Suppl. 201, 431 (1980).

7.- T.R. ANANTHARAMAN, H.L. LUO and W. KLEMENT, Nature, 210, 1040 (1966);
P. DUWEZ, R.H. WILLENS and W. KLEMENT, J.Appl.Phys. 31, 1137 (1960).

8.- P. MANGIN, G. MARCHAL, C. MOUREY and C. JANOT, Phys.Rev.B 21, 3047 (1980).

9.- U. MIZUTANI and T. YOSHIDA, to be published in Proceedings of the Fourth Int.Conf. on Rapidly Quenched Metals, Sendai, Japan, 1981.

10.- N. NGUYEN VAN, M-L. THEYE and S. FISSON, J.Physique 41, C8-489 (1980).

11.- J.M. ZIMAN, Phil.Mag. 6, 1013 (1961).

12.- G. BUSCH and H.J. GUNTHERODT, Solid State Phys. eds H. EHRENREICH, F. SEITZ and D. TURNBULL, Vol. 29 (Academic Press, New York, 1974) p. 235.

13.- P.J. COTE and L.V. MEISEL, Phys.Rev.Lett. 39, 102 (1977);
L. V. MEISEL and P.J. COTE, Phys.Rev. B 17, 4652 (1978).

14.- S.R. NAGEL, Phys.Rev. B 16, 1694 (1977).

15.- K. FRÖBÖSE and J. JÄCKLE, J.Phys. F 7, 2331 (1977)

16.- J. HAFNER, E. GRATZ and H-J. GUNTHERODT, J.Physique C8-512 (1980).

17.- U. MIZUTANI, to be published in Proceedings of the Fourth Int.Conf. on Rapidly Quenched Metals, Sendai, Japan, 1981.

18.- T. MIZOGUCHI, N. SHIOTANI, U. MIZUTANI, T. KUDO and S. YAMADA, J.Physique 41, C8-183 (1980).

19.- F. ABELES and M-L. THEYE, Surf.Sci. 5, 325 (1966).

20.- M-M. DUJARDIN and M-L. THEYE, J.Phys.Chem.Solids 32, 2033 (1979).

21.- E. HAUSER, R.J. ZIRKE, J. TAUC, J.J. HAUSER and S.R. NAGEL, Phys.Rev.Lett. 40, 1733 (1978); Phys.Rev. B 19, 6331 (1979).

22.- M-L. THEYE, Phys.Rev. B 2, 3060 (1970).

23.- J. FUKUSHIMA, K. TAMURA, H. ENDO, K. KISHI, S. IKEDA and S. MINOMURA, J.Physique 35, C4-261 (1974).

24.- J.N. HODGSON, Phil.Mag. 6, 509 (1961).

25.- K. TERAKURA, J.Phys.Soc. Japan 40, 450 (1976).

26.- J.R. WILSON, Met. Rev. 10, 381 (1965).

27.- J. RIVORY, Phys.Rev. B 15, 3119 (1977).

28.- C.C. TSUEI, Sol.St.Commun. 27, 691 (1978).

Table I

x_{Ge} (at.%)	20.5	25	26.5	29.5	32	37
ρ_e ($\mu\Omega$-cm)	117.3	129.7	141.2	171.0	126.2	202.5
$\frac{1}{\rho_e} \cdot \frac{d\rho_e}{dT}$ (10^{-5} K^{-1})	+4	-6.2	-5.6	-12.5	-7	-28

d.c. electrical resistivity at 20K ρ_e and its temperature coefficient $\frac{1}{\rho_e} \cdot \frac{d\rho_e}{dT}$ for several Ag-Ge alloys with Ge concentration x_{Ge}.

Table II

	Σ	$\lambda_o \mu m$	$\lambda_\tau \mu m$	$b \mu m$	P	N_{eff}	$\frac{\hbar}{\tau}$ ev
(R,T) fit (3p) $.8 < \lambda < 2\ \mu m$	1.59×10^{-7}	$.144_3$	.630	—	2.49	8.557	1.968
(R,T) fit (3p) $.6 < \lambda < 2\ \mu m$	5.77×10^{-7}	$.130_0$	.617	—	2.80	6.615	2.009
(R,T) fit (3p) $.4 < \lambda < 2\ \mu m$	1.16×10^{-3}	$.115_3$	.639	—	2.39	8.410	1.940
$(\varepsilon_1, \varepsilon_2)$ fit (3p) $.6 < \lambda < 2\ \mu m$	1.61×10^{-1}	$.114_0$	.628	—	2.44	8.603	1.974
(R,T) fit (4p) $.8 < \lambda < 2\ \mu m$	1.57×10^{-7}	$.113_6$	.622	$.028_4$	1.85	8.663	1.993
(R,T) fit (4p) $.4 < \lambda < 2\ \mu m$	1.16×10^{-3}	$.116_8$	.668	.085	-7.44	8.195	1.856

Results of several fits of the (R, T) and (ε_1 , ε_2) data for a Ag-Ge alloy with d = 207 Å and x_{Ge} = 25 at.%.

Table III

	X_{Ge} (at%)	N_{eff} (10^{22} cm^{-3})	n_{eff}	τ_o (10^{-16} sec)	ρ_o ($\mu\Omega$-cm)	ρ_e ($\mu\Omega$-cm)	$\frac{\hbar}{\tau_o}$ (ev)
Ag	20.5	8.58	1.47 (1.61)	3.86	107.1	117.3	1.70
	25	8.60	1.47 (1.75)	3.34	123.8	129.7	1.98
	26.5	9.58	1.63 (1.80)	2.66	139.7	141.2	2.48
	32	13.53	2.27 (1.96)	2.15	122.1	126.2	3.05
Au	24	11.3	1.94 (1.72)	2.86	109	121	2.30
	30	15.1	2.52 (1.90)	2.23	108	125	2.95

Experimental values of the free electron parameters for Ag-Ge and Au-Ge amorphous metallic alloys with different Ge concentrations x_{Ge} : N_{eff} effective number per volume unit; n_{eff} average effective number per atom (the value between parentheses is the computed value-see text-); τ_o optical relaxation time; ρ_o and ρ_e are the optical and electrical resistivity respectively.

FIGURE CAPTIONS

Figure 1 - Schematic diagram of the ultra-high vacuum co-evaporation system.

Figure 2 - Schematic diagram of the spectrophotometer allowing in situ reflectance and transmittance measurements.

Figure 3 - Electrical set-up for measuring small resistance changes.

Figure 4 - Phase-diagram of the Ag-Ge system (after ref.4).

Figure 5 - Electron micrograph (a) and electron diffraction pattern (b) of a Ag-Ge film : d = 205 Å, x_{Ge} = 26.5 at. %, taken at room temperature.

Figure 6 - Densitograms of the electron diffraction patterns taken at room temperature of three Ag-Ge films with Ge concentrations 26.5, 29.6 and 37 at. %; the full-line arrows indicate the main diffraction peaks of crystalline Ag and amorphous Ge; the discontinuous-line arrows indicate peaks which can be attributed to an h.c.p.alloy phase.

Figure 7 - Densitogram of the electron diffraction pattern of a Ag-Ge film with x_{Ge} = 29.6 at. % which has been heated inside the electron microscope; the arrows indicate the main diffraction peaks of crystalline Ag and crystalline Ge; the other peaks can be attributed to an h.c.p. alloy phase.

Figure 8 - Variation of the d.c. electrical resistivity ρ_e versus temperature T from deposition temperature (20K) to room temperature for Ag-Ge films with different Ge concentrations x_{Ge}.

Figure 9 - Experimental values of the d.c. electrical resistivity at deposition temperature ρ_e (a) and of its temperature coefficient $\frac{1}{\rho_e}\frac{d\rho_e}{dT}$ (b) as a function of Ge concentration x_{Ge} for several amorphous metallic Ag-Ge alloys.

Figure 10 - Reflectance R and transmittance T spectra between 0.3 and 0.8 μm (a) and between 0.5 and 2 μm (b), for a Ag-Ge film : d = 207 Å , x_{Ge} = 25 at. % , as-deposited (dots) and annealed at 120K (dashed lines) and 300 K (continuous lines).

Figure 11 - Optical absorption ε_2 / λ versus energy $\hbar\omega$ for amorphous Ag-Ge films with Ge concentrations x_{Ge} = 20.5 (●), 26.5 (◇) 29.5 (Δ) and 32 (o) at.% and for crystalline Ag (dashed line).

Figure 12 - Comparison between the experimental values of T (o) and R (●) and the results of different fits : 3-parameters fit on (R,T) between 0.6 and 2 μm (dashed lines), 3-parameters fit on (ε_1, ε_2) between 0.6 and 2 μm (dashed-dotted lines), 4-parameters fit on (R,T) between 0.6 and 2 μm (continuous lines).

Figure 13 - Comparison between the experimental values of $-\varepsilon_1$ (o) and ε_2 / λ (•) and the results of different fits : 3-parameters fit on (R,T) between 0.8 and 2 μm (dashed lines) and between 0.4 and 2 μm (dashed-dotted lines), 4-parameters fit on (R,T) between 0.6 and 2 μm (continuous lines).

Figure 14 - Values of the reciprocal optical relaxation time $\frac{1}{\tau_o}$ deduced from the real and imaginary parts of the dielectric constant as explained in the text, as a function of energy square $(\hbar\omega)^2$.

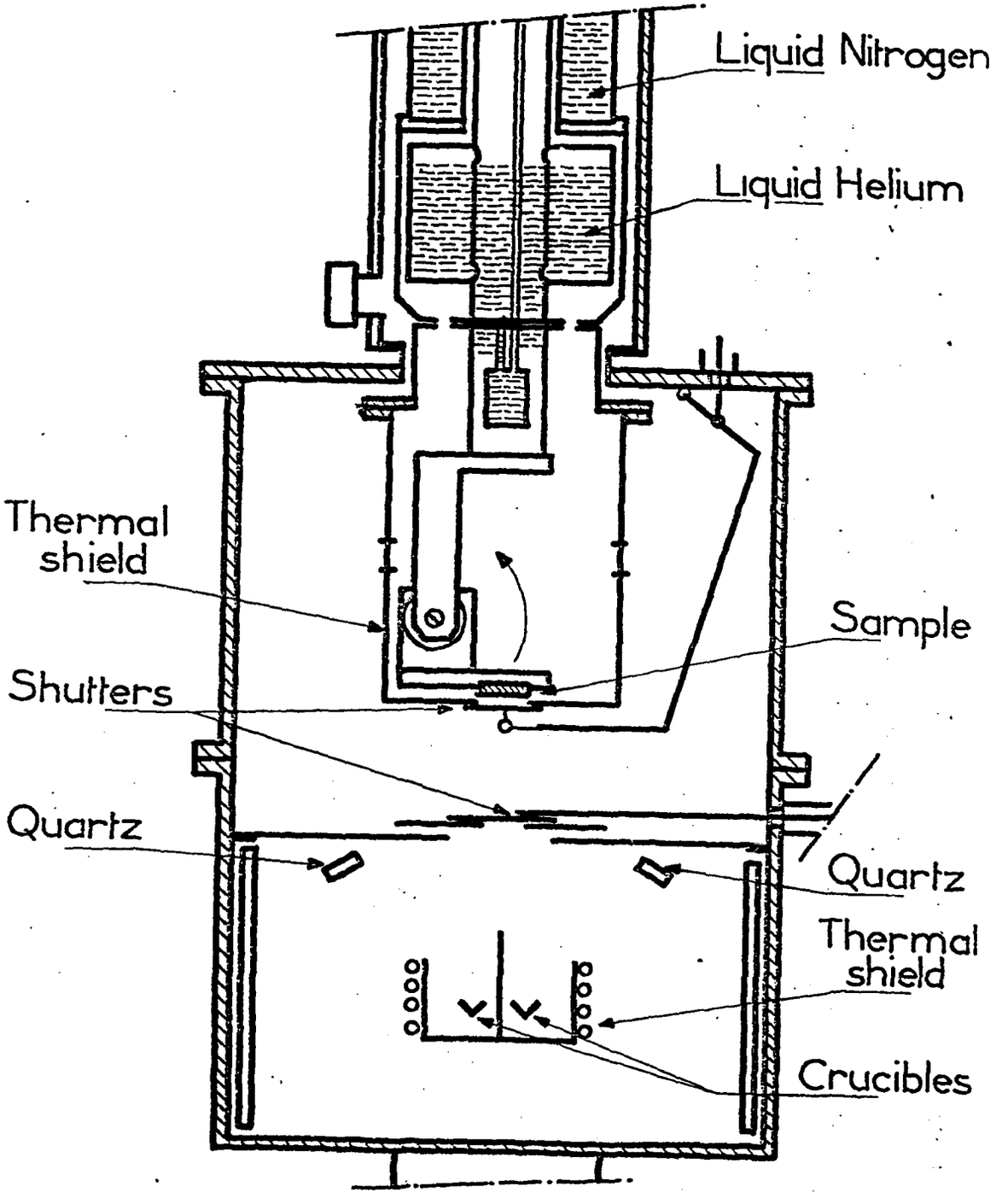
Liquid Nitrogen
Liquid Helium
Thermal shield
Sample
Shutters
Quartz
Quartz
Thermal shield
Crucibles

1

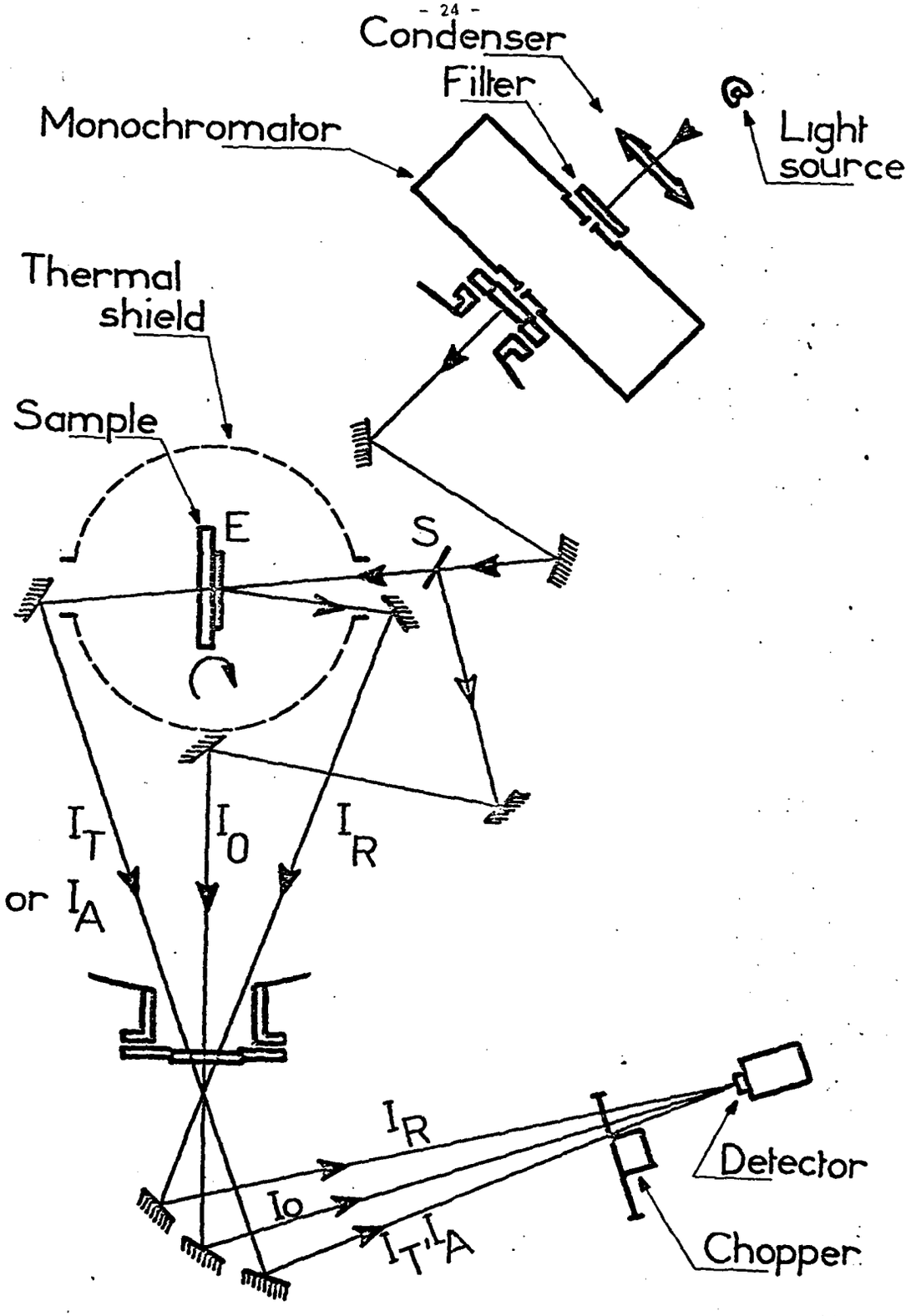
Condenser
Filter
Monochromator
Light source
Thermal shield
Sample
E
S
I_T
or I_A
I_0
I_R
I_R
I_0
I_T I_A
Detector
Chopper

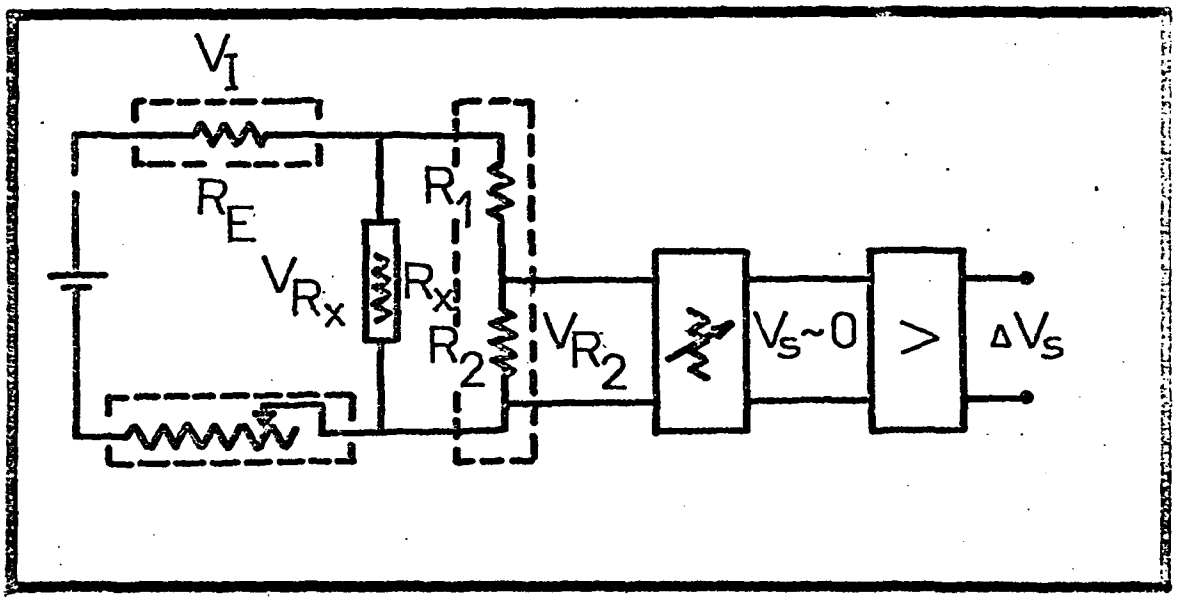
V_I
R_E
V_{R_x}
R_x
R_1
R_2
V_{R_2}
$V_s \sim 0$
>
ΔV_s

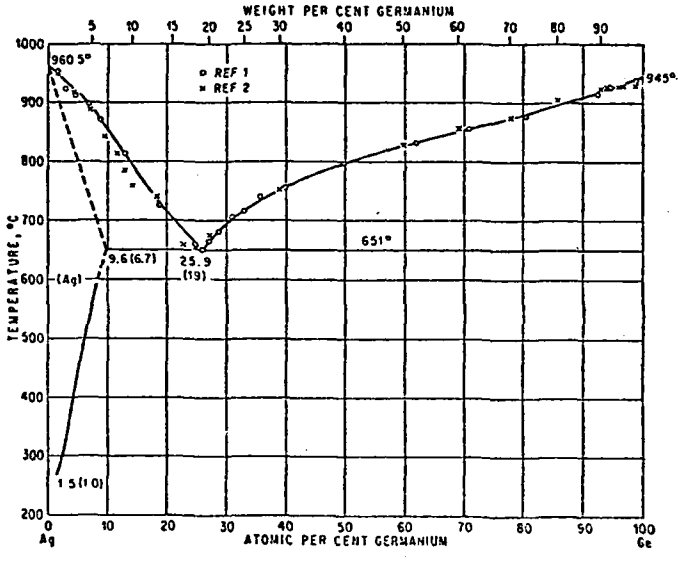
WEIGHT PER CENT GERMANIUM
5 10 15 20 25 30 40 50 60 70 80 90
1000
900
800
700
600
500
400
300
200
TEMPERATURE, °C
960.5°
o REF 1
× REF 2
945°
651°
9.6(6.7)
25.9
(19)
(Ag)
1.5(1.0)
0
Ag
10 20 30 40 50 60 70 80 90
100
Ge
ATOMIC PER CENT GERMANIUM

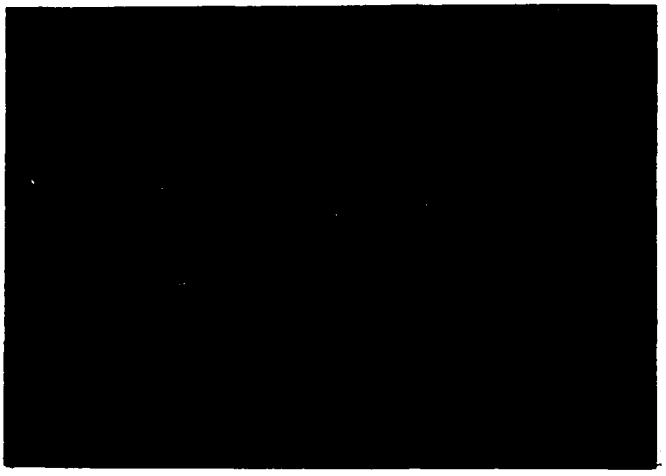

(a)

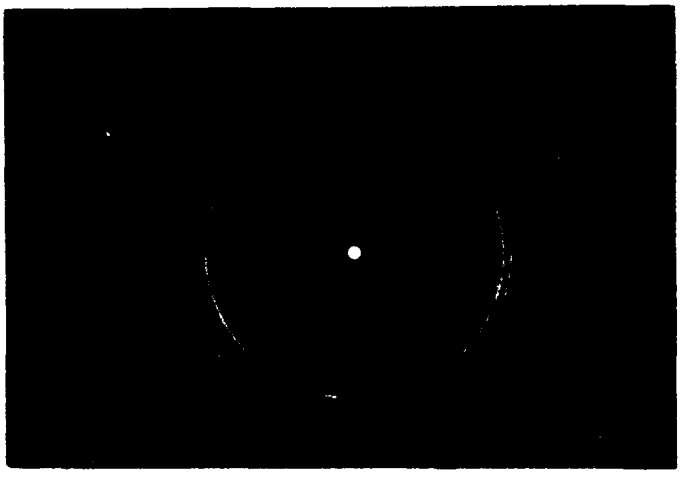

(b)

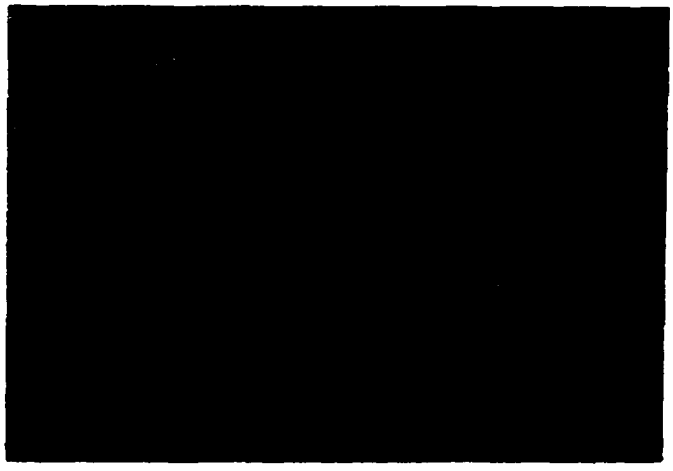

(a)

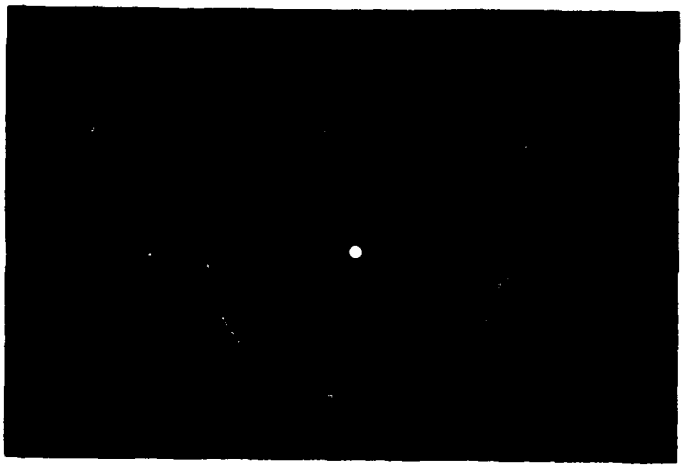

(b)

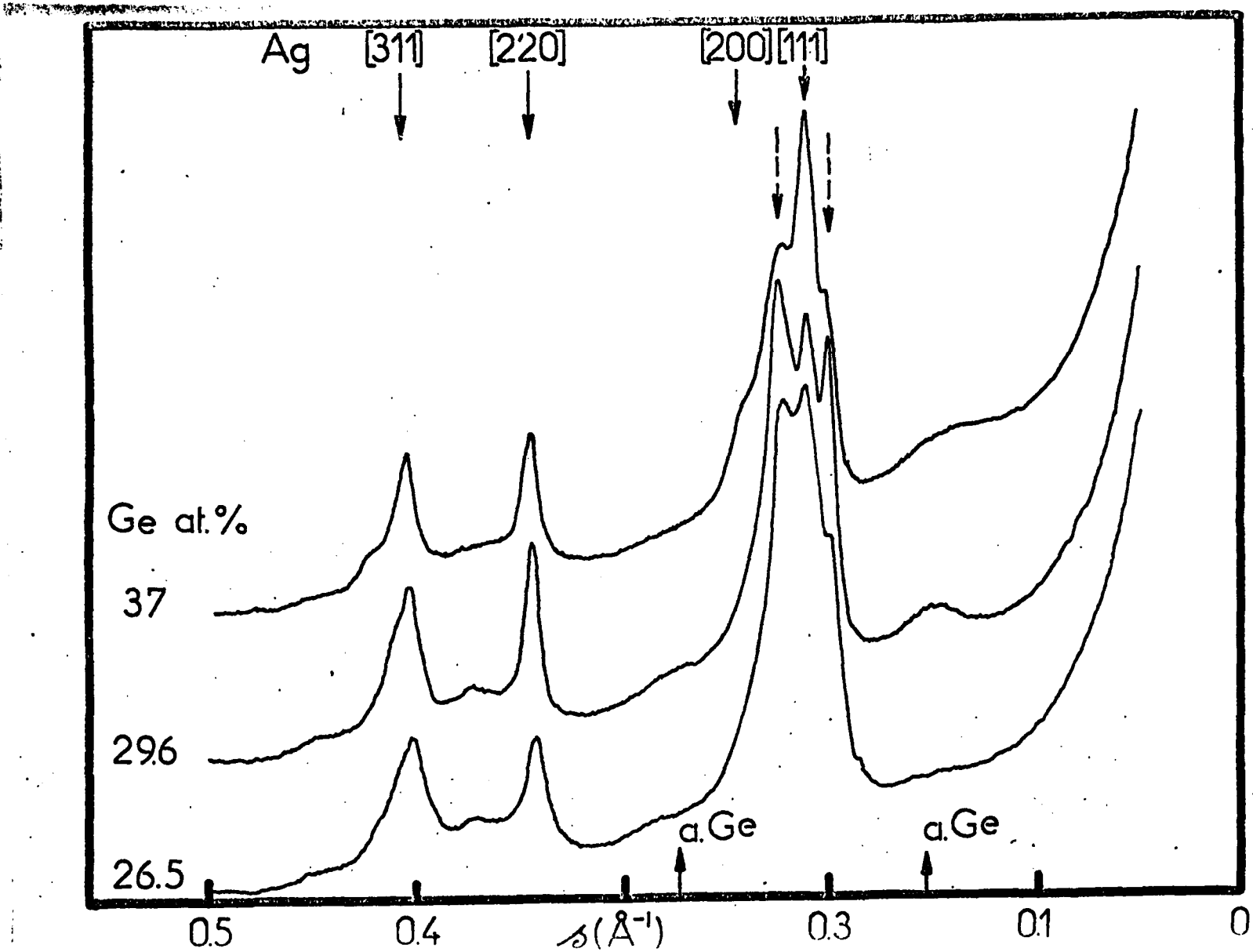
Ag
[311]
[220]
[200]
[111]
Ge at.%
37
29.6
26.5
a.Ge
a.Ge
0.5
0.4
s(Å⁻¹)
0.3
0.1
0
I (a.u.)

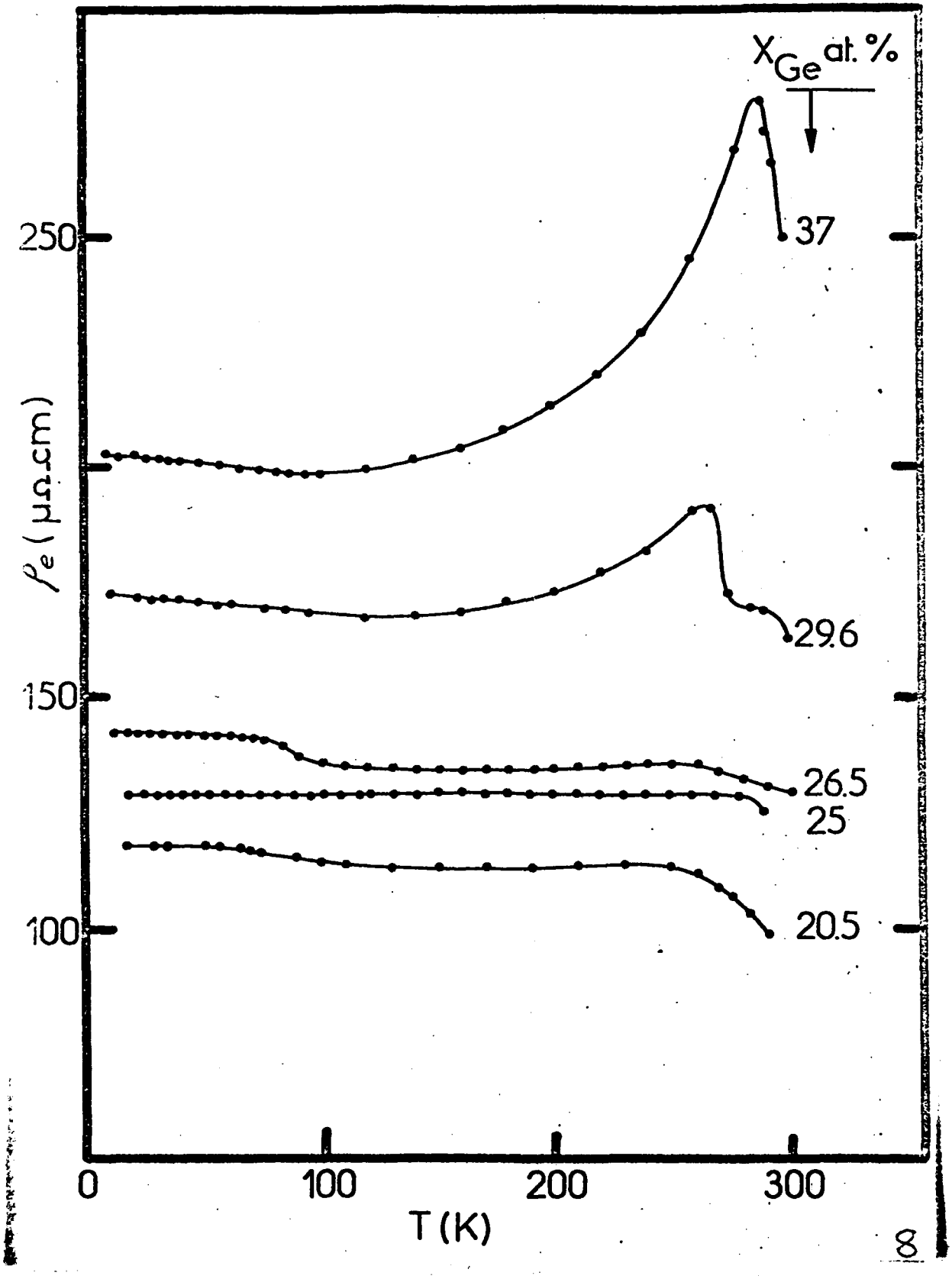
X_{Ge} at. %
37
29.6
26.5
25
20.5
250
150
100
ρ_e (μΩ.cm)
0
100
200
300
T (K)
8

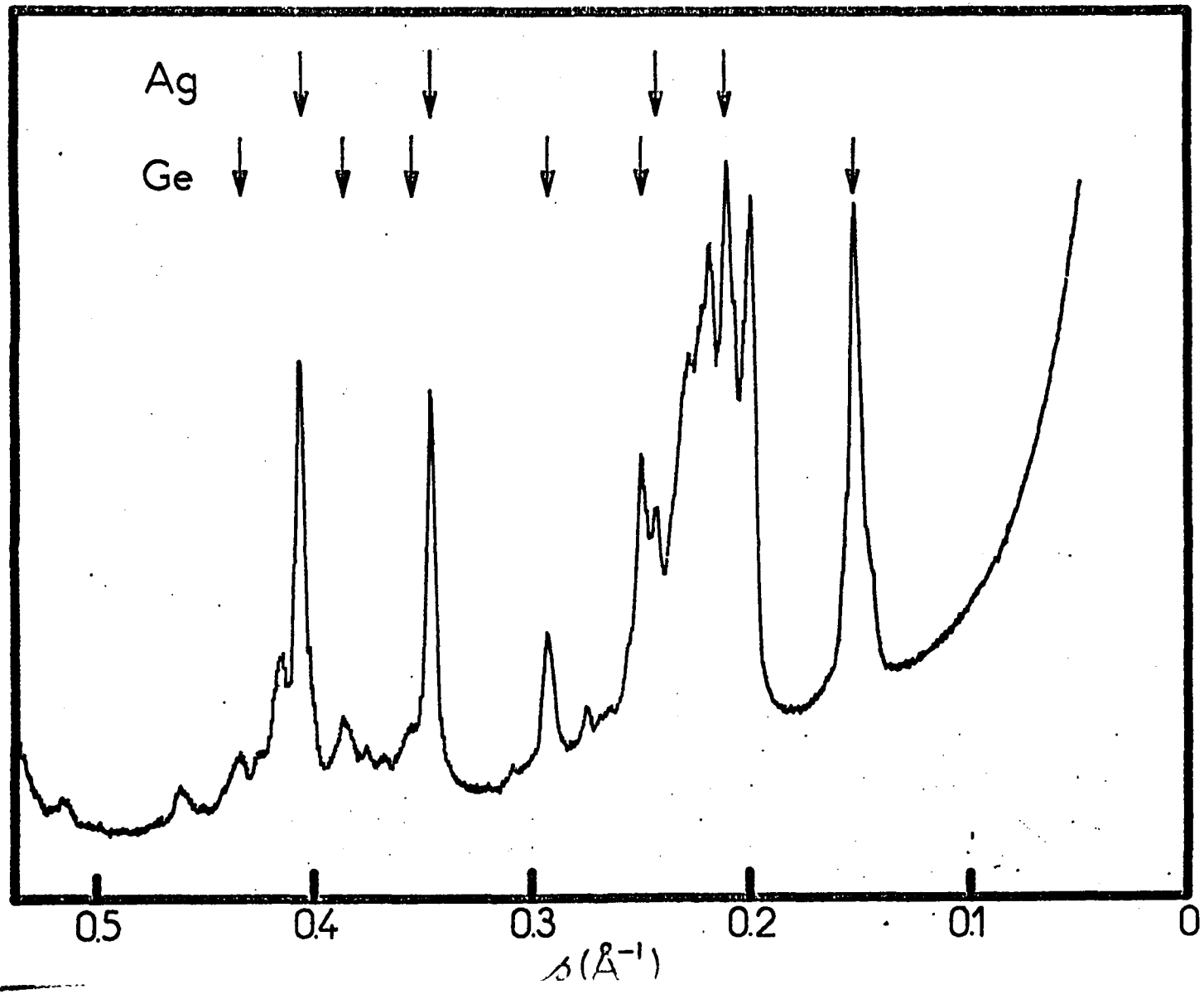
Ag
Ge
0.5
0.4
0.3
0.2
0.1
0
s (Å⁻¹)
I (a.u.)

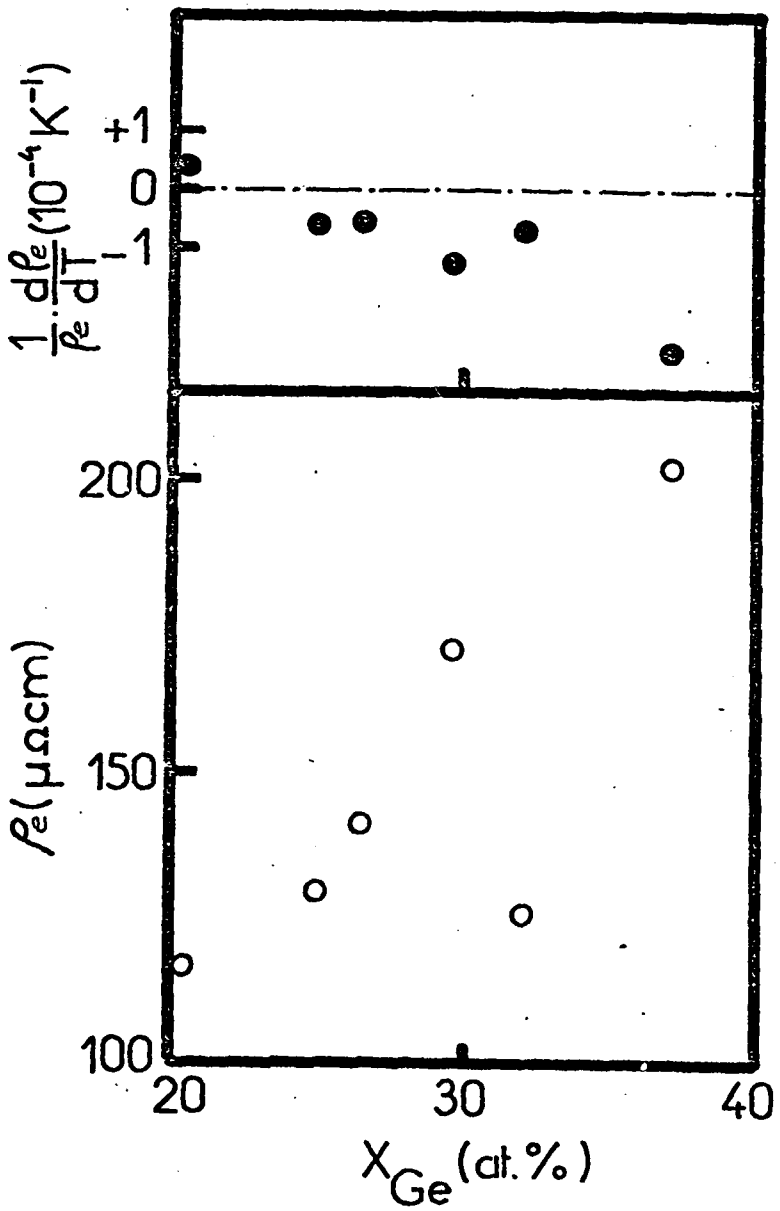
$\frac{1}{\rho_e}\cdot\frac{d\rho_e}{dT}(10^{-4}K^{-1})$
+1
0
-1
(b)
200
150
100
$\rho_e(\mu\Omega cm)$
(a)
20
30
40
X_{Ge} (at.%)

9

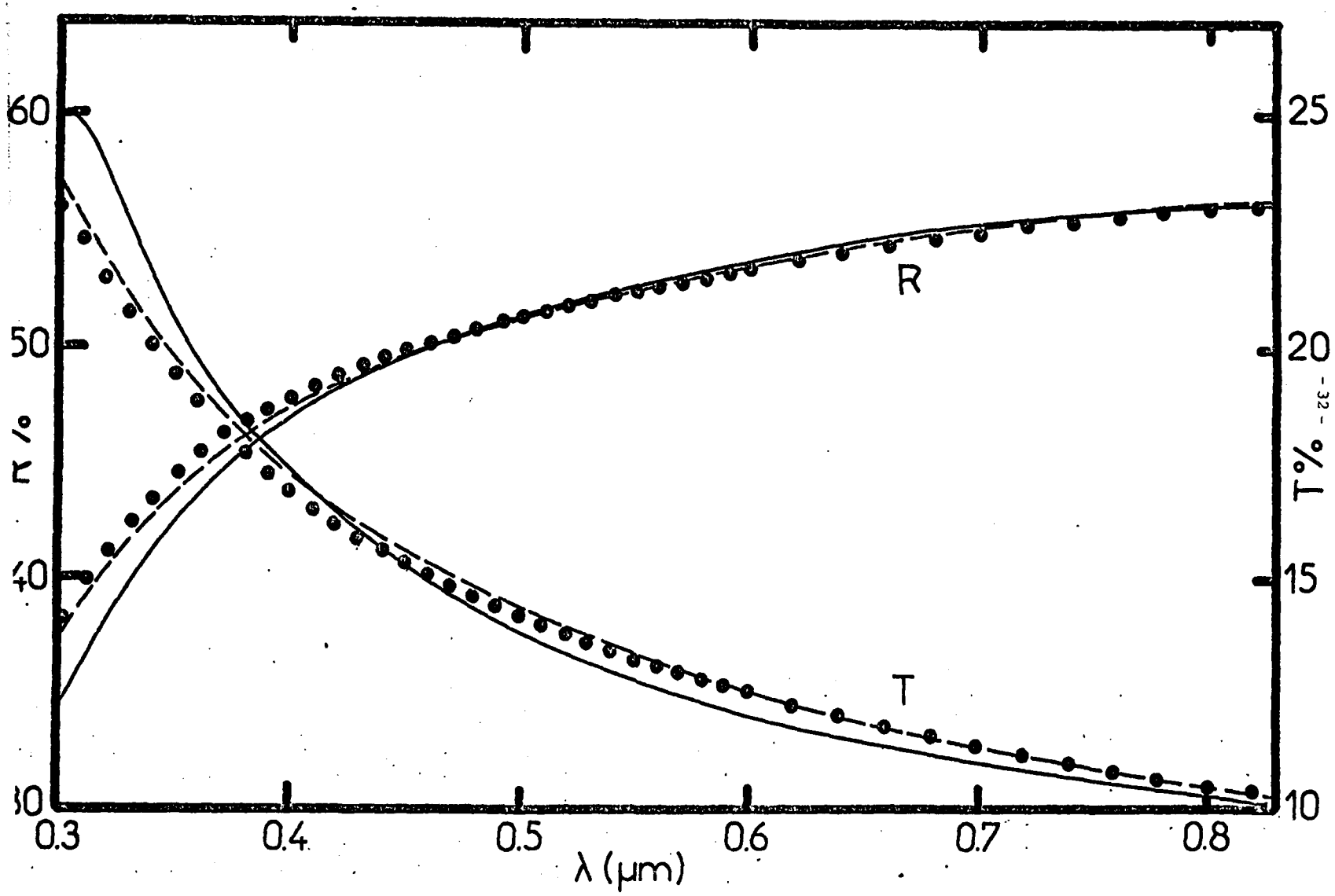
60
50
40
30
R %
25
20
15
10
T %
R
T
0.3
0.4
0.5
0.6
0.7
0.8
λ (μm)

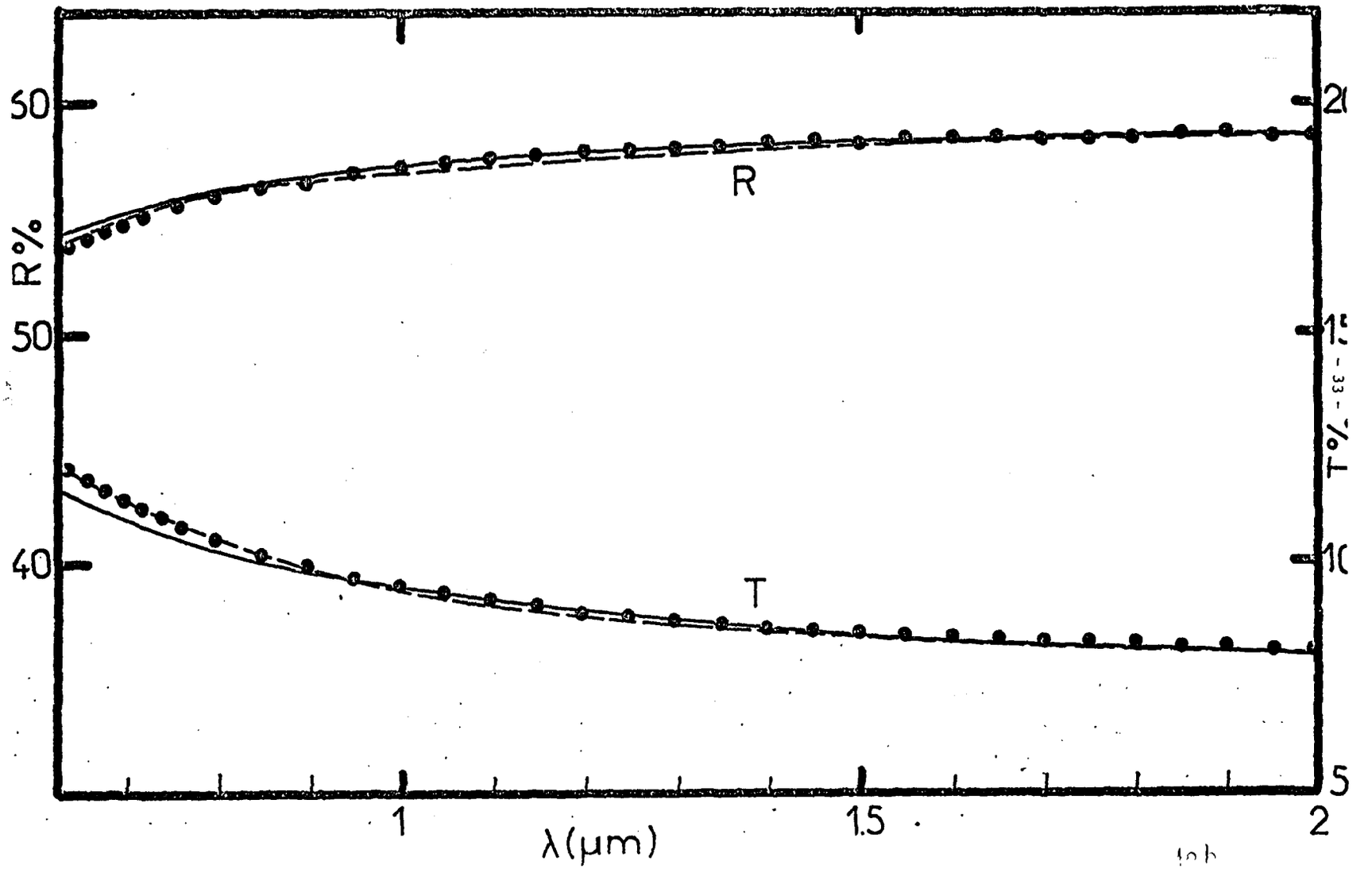
50
R%
50
40
R
T
1
1.5
2
λ(μm)
T%
5

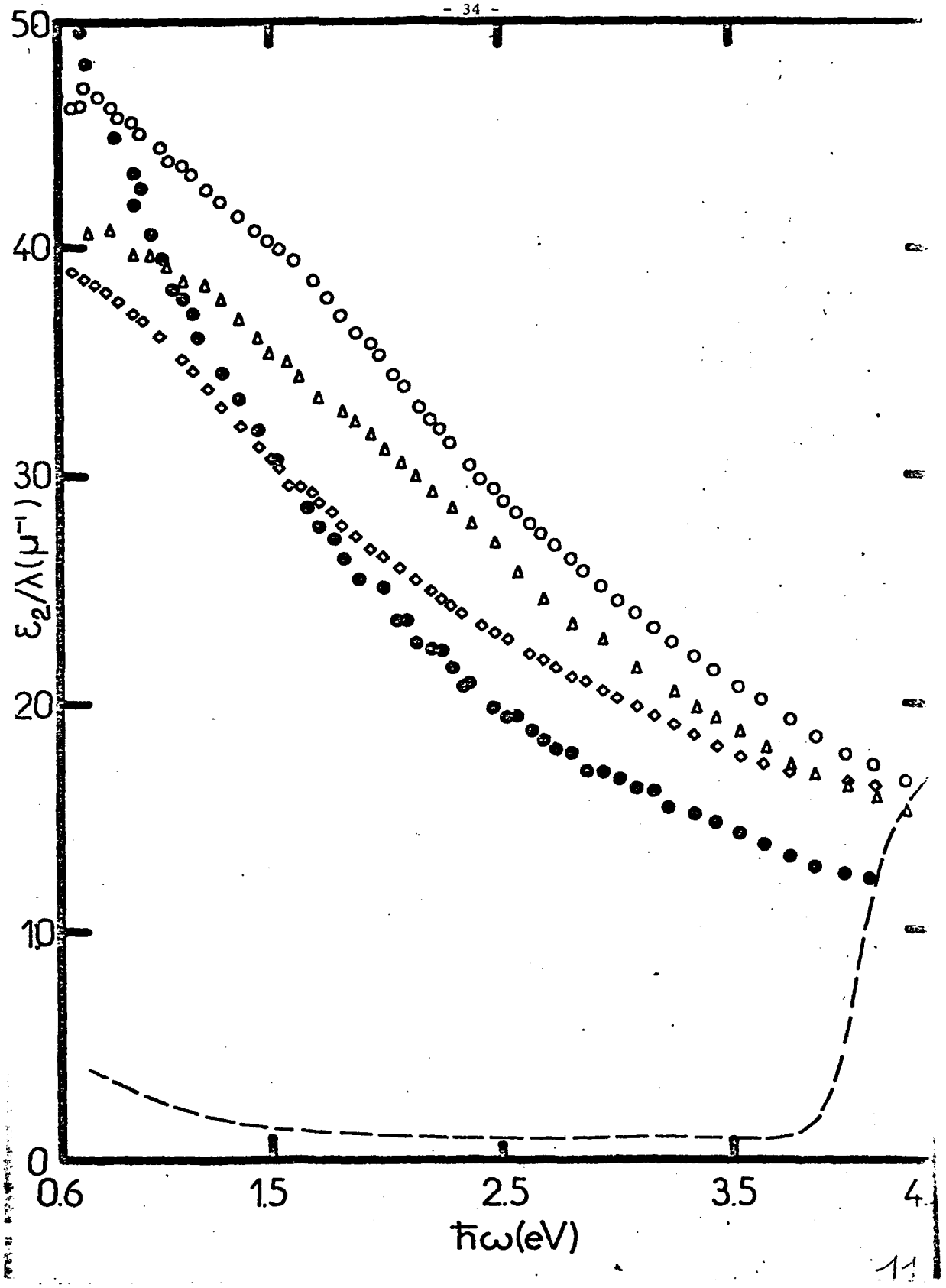
50
40
30
20
10
0
$\varepsilon_2/\lambda(\mu^{-1})$
0.6
1.5
2.5
3.5
4
$\hbar\omega$(eV)

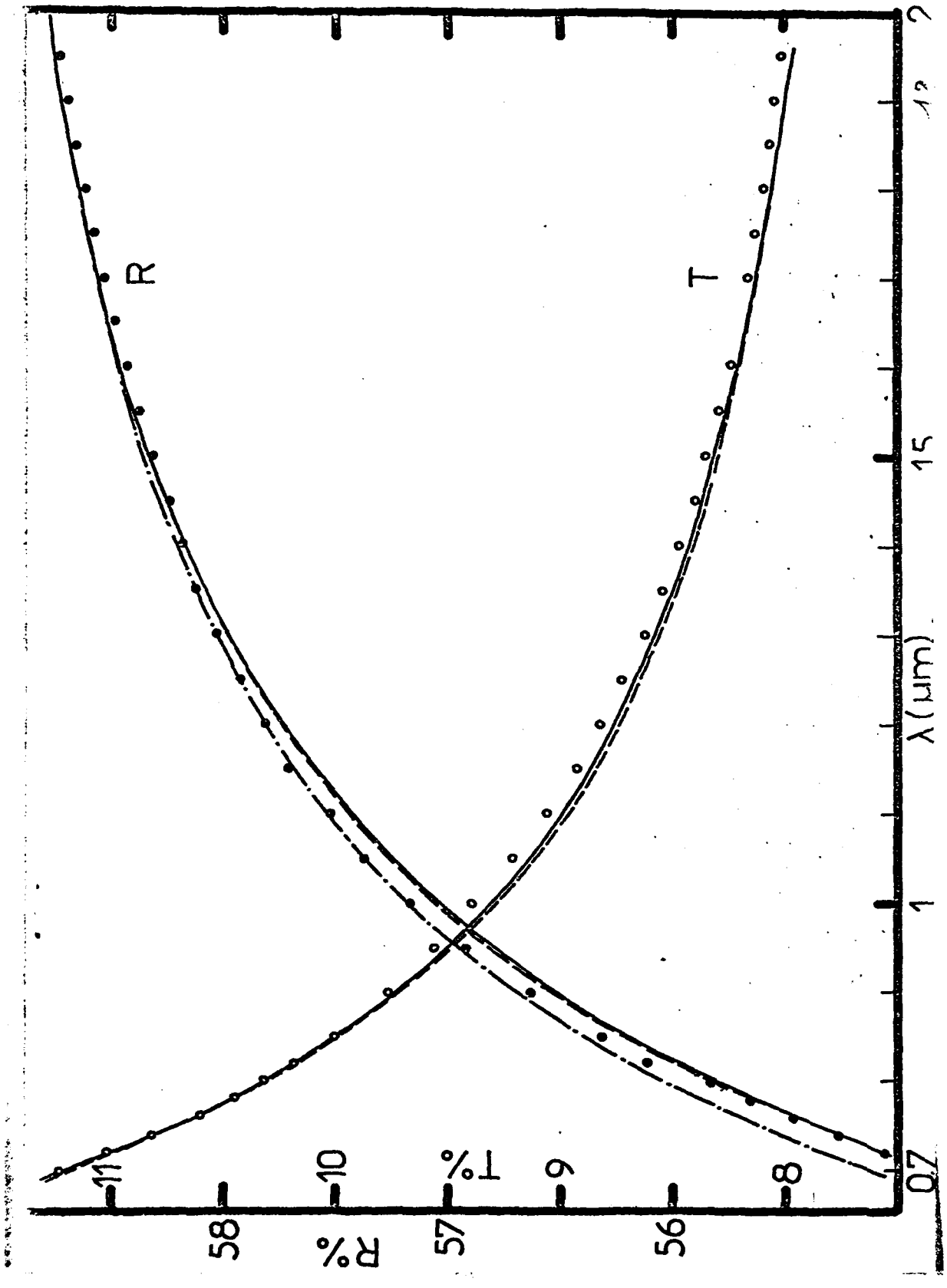
R
T
λ(μm)
0.7
1
1.5
2
R%
58
57
56
T%
11
10
9
8

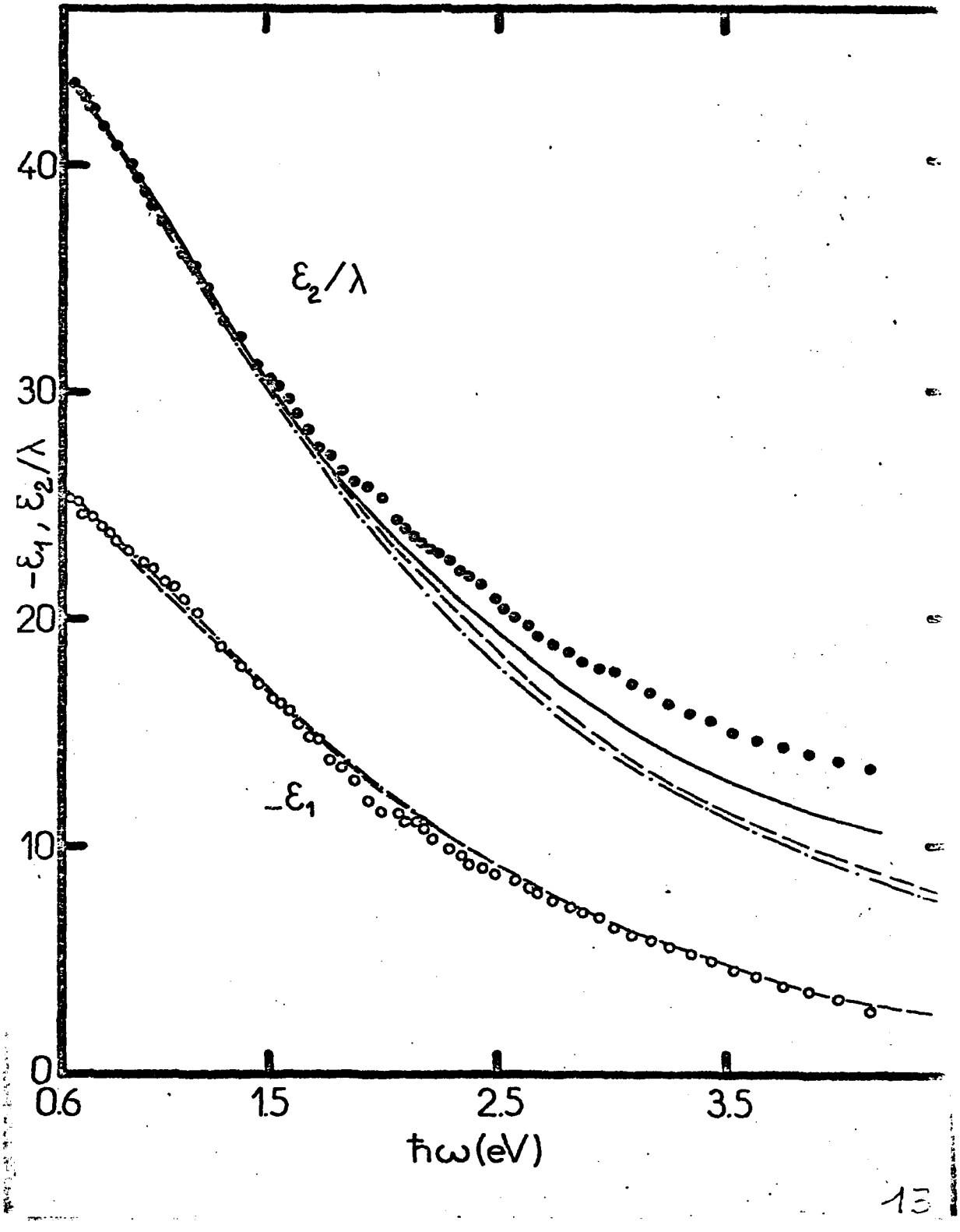
40
30
20
10
0
$-\varepsilon_1, \varepsilon_2/\lambda$
ε_2/λ
$-\varepsilon_1$
0.6
1.5
2.5
3.5
$\hbar\omega$(eV)
13

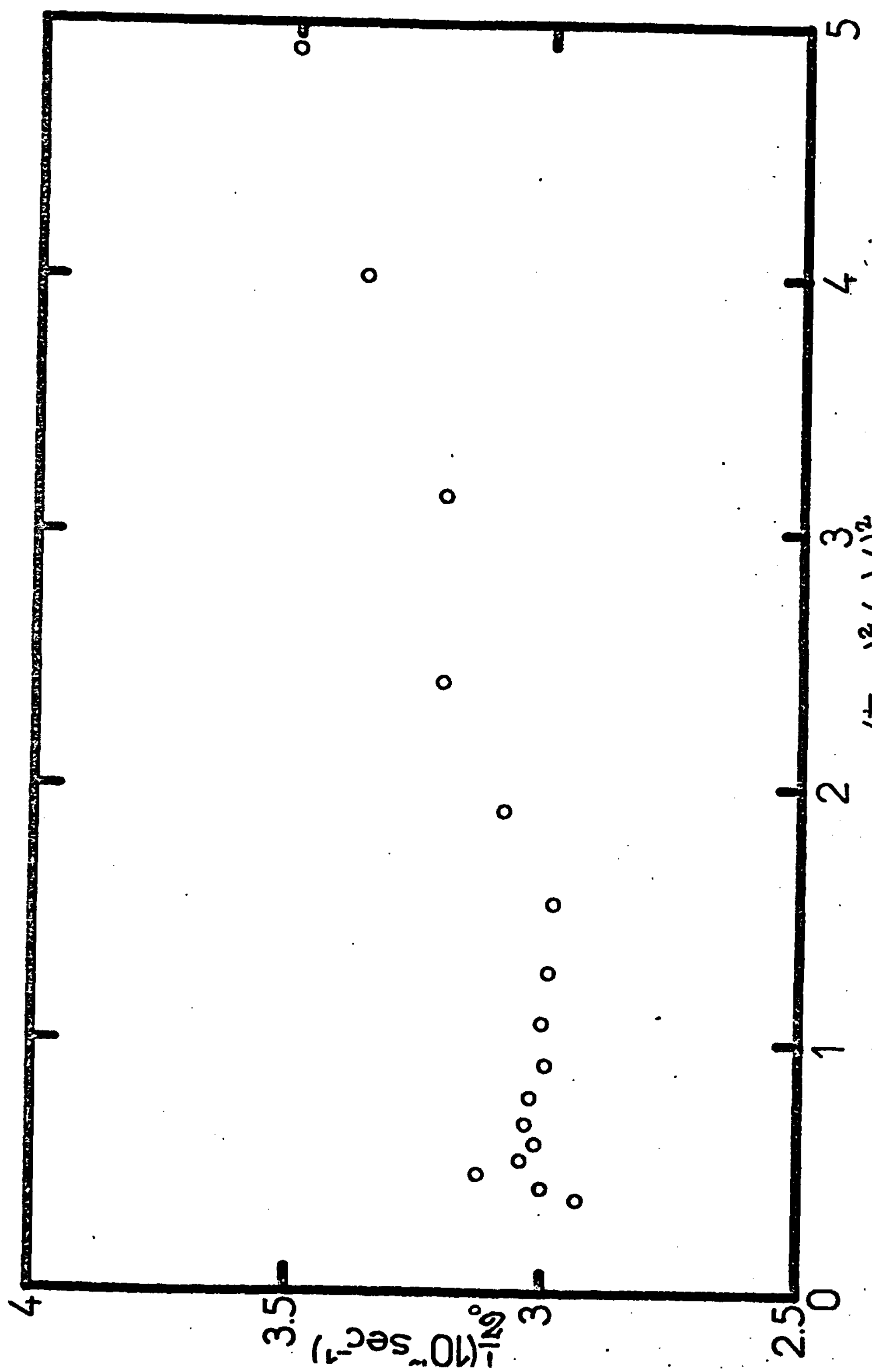
4
3.5
3
2.5
0
1
2
3
4
5
(ħω)² (eV)²